Nonstatistical unimolecular dissociation over a barrier

David H. Mordaunt, David L. Osborn,[a] and Daniel M. Neumark
Department of Chemistry, University of California, Berkeley, California 94720 and Chemical Sciences Division, Lawrence Berkeley Laboratory, Berkeley, California 94720

(Received 6 October 1997; accepted 4 November 1997)

A general formulation is presented to model photodissociation processes in which internal conversion is followed by unimolecular dissociation over an exit barrier; this classification of dissociation mechanism results in a nonstatistical product state distribution. The energy available to products is divided into independent statistical and impulsive energy reservoirs. The statistical reservoir considers direct projections of a vibrational microcanonical ensemble at the transition state (TS) onto product quantum states, conserving vibrational adiabaticity and angular momentum. The impulsive reservoir represents the energy released in passing from the TS to products; this reservoir is treated assuming sudden dissociation of the zero-point TS wave function using a combination of Franck-Condon and impulsive models. We derive the statistical adiabatic impulsive model, which convolutes these two energy reservoirs, to predict the product translational energy distribution for nonstatistical dissociation over a barrier. Two test cases are modeled and compared with experimental data: unimolecular dissociation of acetyl radicals and photodissociation of vinoxy radicals via the $\tilde{B}\ ^2A''$-$\tilde{X}\ ^2A''$ band. © *1998 American Institute of Physics.*
[S0021-9606(98)02106-0]

I. INTRODUCTION

In many examples of photodissociation, electronic excitation is followed by internal conversion to the electronic ground state and subsequent unimolecular dissociation.[1–4] If there is an exit barrier on the ground state surface, the resulting product energy distribution generally cannot be reproduced by statistical models for chemical reactions even if the ground state complex persists for many vibrational periods. In this article, we propose a simple model that predicts the nonstatistical product translational energy distribution that arises when there is an exit barrier on the ground state surface.

Internal conversion of the initially prepared excited state yields a microcanonical ensemble of vibrational states on the ground state potential energy surface (PES). In the absence of a barrier, unimolecular dissociation of a microcanonical ensemble can be treated classically in terms of Liouville's theorem; a system with an equilibrium distribution in one part of phase space evolves with an equilibrium distribution in other parts of phase space, so that all parts of an undivided phase space are in equilibrium. The consequence of this is that energy is randomized with equal probability among all vibrational levels (up to the fixed excitation energy) and all product states have an equal probability of being populated. There is an abundance of well-established theories to predict product quantum state distributions for microcanonical ensemble unimolecular dissociation in the absence of a barrier, e.g., prior distributions,[5] phase space theory (PST)[6] and the statistical separable ensemble method.[7]

The presence of a barrier defines an implicit transition state (TS) at the saddle point of the PES. Following transition state theory,[8] the TS forms a dynamical bottleneck for molecular trajectories dividing phase space into two distinct regions: reactant and products. The product vibrational and rotational distributions resulting from a simple sudden impulsive force at the TS (i.e., a sudden photodissociation) are generally interpreted in terms of Franck-Condon mapping[9] and impulsive models[10] respectively. Whilst these distributions may be valid at energies close to the barrier height, they become more problematic at large excess energies.

Only a few theories address the product quantum state distribution for nonstatistical unimolecular dissociation over a barrier. For dissociation energies in close proximity to the barrier height, the statistical adiabatic channel model (SACM)[11] is generally utilized; Chen and Moore[12] have also developed a modified impulse model to rationalize triplet ketene dissociation at the TS. For energies in large excess of the barrier height more simplistic models are used. As early as 1974, Berry[13] proposed the ''bootstrap'' model to describe partial vibrational inversion. Later, Zamir and Levine[14] related this type of nonstatistical behavior to surprisal theory in the form of a ''sum rule.'' More recently, Sonobe *et al.*,[15] Gejo *et al.*,[16] and North *et al.*[17] have proposed statistical-impulse models to explain the low degree of vibrational excitation and the high degree of translational energy in photoproducts.

The common theme to all of these models[13–17] is that the total energy available to products is partitioned into two reservoirs: first, the available energy in excess of the barrier, and second, the barrier height with respect to the exit valley. The treatment of each energy reservoir is dependent on the respective theories. In this article we derive a general framework, the statistical adiabatic impulse (SAI) model, which

[a]Present address: JILA, National Institute of Standards and Technology and University of Colorado, and Department of Chemistry and Biochemistry, University of Colorado, Boulder, CO 80309-0440.

combines statistical and sudden theories expanding on previous models of this type. No adjustable parameters are used in the SAI model, although it does require the TS energy, geometry and vibrational frequencies, all of which are typically obtained from *ab initio* calculations. A brief account of this model has been previously published.[18]

Unimolecular dissociation of acetyl radicals and photodissociation of vinoxy radicals via the $\tilde{B}\ ^2A''$-$\tilde{X}\ ^2A''$ band are examples of the type of processes we can treat with the SAI model. In both cases, experimental studies[17–21] have determined that nonstatistical product state distributions are produced; experiment[18–20,22,23] and theory[18,23] have also demonstrated the existence of exit barriers for dissociation. Our SAI model simulates product state distributions for these two molecular systems and the main factors influencing these distributions are determined.

This article comprises four sections. In Section II, we describe the theoretical basis of our SAI model. Section III describes the physical processes involved in unimolecular dissociation of a microcanonical ensemble over a barrier. The SAI model predicts the product translational energy distributions for acetyl and vinoxy dissociation and is compared with experimental results. Finally, the conclusions are summarized in Section IV.

II. THE STATISTICAL ADIABATIC IMPULSIVE (SAI) MODEL

In this section we formulate the theoretical basis of the SAI model, to provide a general framework for modeling and interpreting nonstatistical unimolecular dissociation over a barrier. The SAI model describes the molecular behavior of unimolecular dissociation of a microcanonical ensemble through a TS, and predicts the resultant product translational energy distribution. We utilize a simple approach combining both statistical and sudden unimolecular dissociation theories, building on previous nonstatistical theories.[13,17]

Our initial assumption is that a microcanonical ensemble of vibrational modes is formed on the ground state PES, which asymptotically correlates with products. Internal conversion from the initially prepared excited electronic state will result in a microcanonical ensemble on the ground state PES.

Our second main assumption is that the total energy available to products ($E^{AVAIL}=h\nu-D_0$) is divided into two independent energy reservoirs, Figure 1. The statistical reservoir is the available energy in excess of the TS, i.e., $E^{STAT}=E^{AVAIL}-E^{TS}$, where E^{TS} is the zero-point level of the transition state. The sudden reservoir represents the energy of the TS relative to the ground state energy of the products, i.e., $E^{IMP}=E^{TS}$. The energy within each reservoir remains constant throughout dissociation, i.e., no energy is allowed to flow between the two reservoirs. This follows the same approach as the previous models addressing dissociation over a barrier.[13–17] Implicit in this assumption is that the reaction is electronically adiabatic (i.e., the Born-Oppenheimer separation of electronic motion from internuclear motion is valid) in the vicinity of the TS. This is particularly pertinent as a TS can arise from the avoided crossing of electronic surfaces of the same electronic symmetry.

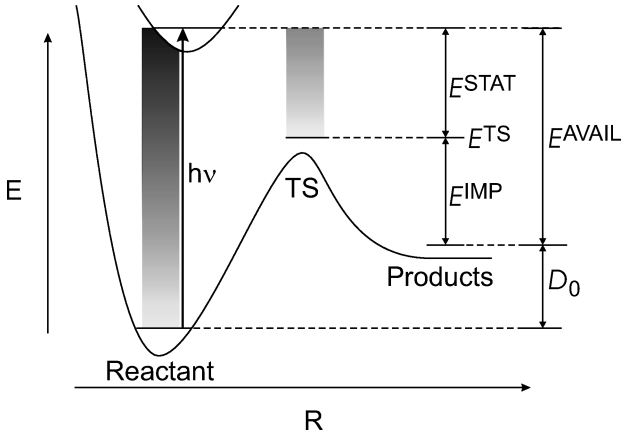

FIG. 1. Schematic diagram illustrating the division of the energy available to products ($E^{AVAIL}=h\nu-D_0$) into two independent energy reservoirs defined in the SAI model: the statistical reservoir ($E^{STAT}=E^{AVAIL}-E^{TS}$) and the sudden reservoir ($E^{IMP}=E^{TS}$).

A. Statistical reservoir

Within the statistical reservoir, we assume that the TS is in equilibrium with the reactant region of phase space where the microcanonical ensemble is formed; thus in accordance with Liouville's theorem, a microcanonical ensemble of vibrational levels exists at the transition state. Once beyond the TS the molecule rapidly dissociates into products; an equilibrium does *not* exist between the TS and products—hence two distinct regions of phase space are defined.

The contribution from the statistical reservoir to the product internal energy distribution $P^{STAT}(E'_{INT})$ is calculated assuming that the microcanonical ensemble at the TS maps directly into products degrees of freedom. The projection from the TS to products is assumed to be vibrationally adiabatic as in the SACM,[11] i.e., vibrational quantum numbers at the TS are preserved through dissociation to product degrees of freedom. This assumption is justified, as the fragments will separate rapidly after transversing the TS region. Hence it is necessary to correlate each TS vibrational mode with a particular product vibrational (V), rotational (R) or translational (T) degree of freedom. This correlation is based upon the *ab initio* vibration eigenvectors calculated at the TS and products. For example in the CH_3CO system, eleven vibrational modes exist at the TS; seven correlate with V, two with R, and two with T product degrees of freedom.

Each accessible TS vibrational level is described by a specific quantum number for each TS mode, such that its energy is defined by,

$$E'^{TS}_{INT}=E'_V+E'_R+E'_T, \tag{1}$$

where E'_V,E'_R,E'_T are the subdivision of the internal energy into TS modes that correlate with products V, R and T. The energy of each subdivision in Eq. 1 is given by

$$E'_{V,R,T}=\sum_{1}^{S_{V,R,T}} n_{V,R,T}\nu^{TS}_{V,R,T}. \tag{2}$$

$S_{V,R,T}$ denotes the number of TS vibrational degrees of freedom, $n_{V,R,T}$ are the vibrational quantum numbers and $\nu^{TS}_{V,R,T}$ the TS frequencies which correlate with product V, R or T.

The product state distributions are calculated in terms of internal energy. Product vibrational energy ($\Sigma_1^{S_V} n_V \nu_V^{prod}$) is simply calculated substituting the product frequency (ν_V^{prod}) for the correlating TS frequency (ν_V^{TS}), preserving the vibrational quantum number in Eq. 2. The vibrational energy deficit or surplus for each level is assumed to flow freely between V and T degrees of freedom, with the restriction that the maximum product V energy is $E'_V+E'_T$. The remaining energy partitioned into T at the TS is subject to conservation of angular momentum and will result in T and R of the products; this is dealt with in the same manner as the partition between T and R in the impulsive reservoir, Sect. II B.

Energy in ν_R^{TS} modes (E'_R) correlates with product R; conservation of angular momentum also implies that some of this energy is partitioned into product T. The partition of this energy between R and T is calculated utilizing PST[6] for the case of a tight TS state, yielding a rotational energy distribution. The rotational constants are calculated assuming the zero-point TS geometry. The product internal energy distribution for each TS vibrational level is the sum of the vibrational energy, the PST rotational energy distribution and rotational energy from conservation of angular momentum. The final product internal energy distribution for the statistical reservoir $P^{STAT}(E'_{INT})$ is the summation over product internal energy distributions for each energetically allowed TS vibrational level.

It is worth emphasizing that the product state distribution of the fragments from this reservoir is not strictly statistical, i.e., the energy is *not* fully randomized among product states. Rather, energy is statistically distributed at the tight TS and evolves adiabatically to the product states.

B. Impulsive reservoir

The impulsive reservoir is treated as a sudden unimolecular dissociation of the zero-point TS wave function, within the harmonic oscillator and rigid rotor approximations. The vibrational energy distribution of the products, $P_V^{IMP}(E''_{INT})$, is determined by Franck-Condon projection of the zero-point TS wave function, $\Pi_V|\nu_V^{TS}\rangle$, onto the asymptotic product wave functions, $\Pi_{\nu'}|\nu_{\nu'}^{PROD}\rangle$ with a product internal energy of E_{INT}^{PROD},[24]

$$P_V^{IMP}(E''_{INT}) \propto \sum_V \sum_{\nu'} |\langle \nu_V^{TS}|\nu_{\nu'}^{PROD}\rangle|^2 \cdot \delta(E''_{INT}-E_{INT}^{PROD}). \tag{3}$$

For each product vibrational state, the remaining energy in the sudden reservoir is partitioned between T and R degrees of freedom, using a rigid impulsive model based on the TS geometry and ν_R^{TS} zero-point motion. The fraction of impulsive rotational energy, E_R^{IMP}, over the available energy in the impulsive reservoir ($E^{IMP}-E_V^{IMP}$), is given by[10,12,17]

$$f_R = \frac{E_R^{IMP}}{E^{IMP}-E_V^{IMP}} = 1 - \frac{1}{1+\dfrac{\mu_A b_A^2}{I_A}+\dfrac{\mu_B b_B^2}{I_B}}. \tag{4}$$

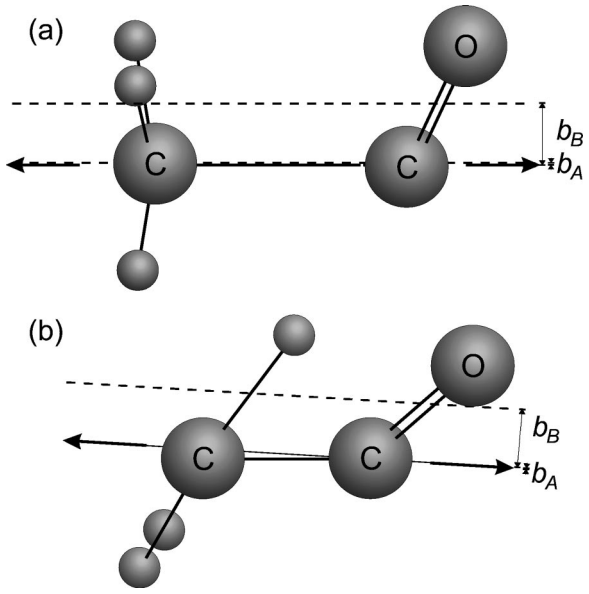

FIG. 2. TS geometries for (a) acetyl, and (b) vinoxy molecular systems. The impulsive force (arrow) and the impact parameters (b_A and b_B) are indicated for CH_3 and CO fragments with respect to the dissociating bond.

The reduced masses, impact parameters and moments of inertia of products are denoted by μ_A, μ_B, b_A, b_B, I_A and I_B for the two fragments A and B, e.g., Figure 2. The TS geometry will define the most probable value of f_R; in order to obtain a continuous distribution over internal energy a probability distribution, $I_R(f_R)$, is obtained by considering the TS zero-point wave function, $|TS_{Z.P.}\rangle$,[12] such that

$$I_R(f_R) = \frac{\langle TS_{Z.P.}|f_R|TS_{Z.P.}\rangle}{\langle TS_{Z.P.}|TS_{Z.P.}\rangle}. \tag{5}$$

The internal energy $P^{IMP}(E''_{INT})$ distribution for the sudden reservoir is the sum of the R internal energy, predicted by the impulsive model, for each combination of vibrational product states, weighted by their FC projection factors,

$$P^{IMP}(E''_{INT}) = \int_0^{E''_{INT}} P_V^{IMP}(E_V^{IMP}) \int_0^{E''_{INT}E_V^{IMP}} I_R\left(\frac{E_R^{IMP}}{E''_{INT}E_V^{IMP}}\right) dE_R^{IMP} dE_V^{IMP} \times \delta(E''_{INT}-E_V^{IMP}-E_R). \tag{6}$$

The $P^{IMP}(E''_{INT})$ distribution is independent of excitation energy, as the energy of this reservoir is defined by the constant energy of the TS.

C. Translational energy distributions

Finally, we bring these reservoirs together to yield the overall internal energy $P(E_{INT})$ distribution. Roughly speaking, the sudden reservoir describes the unimolecular dissociation of the zero-point wave function accounting for the TS geometry. The statistical reservoir describes the adiabatic projection of the TS microcanonical ensemble onto product degrees of freedom, irrespective of the TS geometry. Convolution of the statistical and sudden distributions yields,

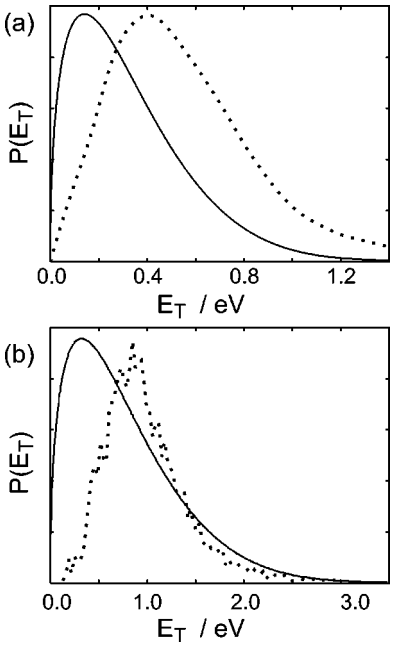

FIG. 3. Acetyl and vinoxy radicals are examples for nonstatistical unimolecular dissociation. Comparison of experimentally determined $P(E_T)$ distributions (dashed) (Refs. 21, 18) to calculated prior distributions (solid) for unimolecular dissociation of (a) the acetyl radical at 1.95 eV, and (b) the vinoxy radical at 3.57 eV.

$$P(E_{INT}) = \int_0^{E^{IMP}} P^{IMP}(E''_{INT}) \cdot P^{STAT}(E_{INT} - E''_{INT}) dE''_{INT}. \tag{7}$$

The translational energy $P(E_T)$ distribution is obtained by expressing the function $P(E_{INT})$ in terms of $E_T = E^{AVAIL} - E_{INT}$:

$$P(E_T) = \int_0^{E^{IMP}} P^{IMP}(E''_{INT}) \cdot P^{STAT}(E^{AVAIL} - E_T - E''_{INT}) dE''_{INT}. \tag{8}$$

We emphasize that the SAI model contains no adjustable parameters and conserves energy and angular momentum in each separate reservoir and therefore for the overall process.

III. APPLICATIONS OF THE SAI MODEL

In this section we apply the SAI model to predict experimental $P(E_T)$ distributions for the unimolecular dissociation of metastable acetyl radicals, resulting from the photolysis of acetyl halides,[19–21] and direct measurements of the photodissociation of vinoxy radicals from fast radical beam studies.[18] The experimental $P(E_T)$ distributions for unimolecular dissociation of acetyl radicals with an average internal energy of 1.95 eV[21] and vinoxy radicals with an internal energy of 3.57 eV[18] are compared to calculated prior distributions[5] in Figure 3. There is a clear difference between the experimental (dashed) and prior (solid) distributions demonstrating the nonstatistical nature of the two product state distributions. In both cases, a larger fraction of the available energy is partitioned into product translational energy than predicted by the prior distributions. The intensity of the experimental $P(E_T)$ distributions increase from zero translational energy to maxima at $E_T \sim 0.37$ and 0.95 eV for acetyl and vinoxy radicals, respectively, and thereafter decrease with increasing E_T. The prior distributions for acetyl and vinoxy peak at considerably lower translational energies: $E_T \sim 0.15$ and 0.25 eV, respectively. For both radicals, experiment[18–20,22,23] and theory[18,23] indicate the existence of exit barriers for dissociation, as shown in Figures 4 and 5. Thus these are good candidates to test the SAI model.

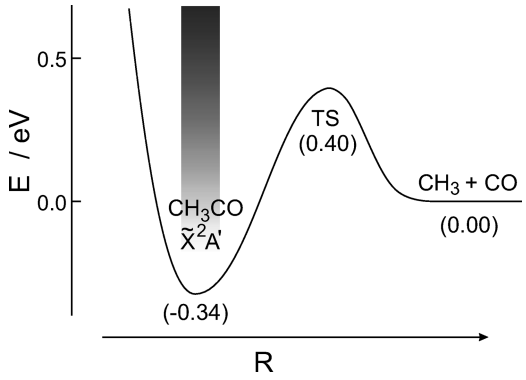

FIG. 4. Schematic potential energy surface of the acetyl radical system leading to CH_3 and CO products, derived from Ref. 18. All energies are in eV, including zero-point energies and are relative to the product minimum.

A. Unimolecular dissociation of acetyl radicals

Several experimental studies have examined the fragmentation of the acetyl radical. Photodissociation of acetyl halides (CH_3COX: X=Cl,[19,20] Br,[20] I[21]) and acetone[17] yield metastable internal excited acetyl radicals with a range of average internal energies between 0.69 to 1.95 eV. Subsequent unimolecular decay of these metastable acetyl radicals yield $P(E_T)$ distributions which are all relatively independent of initial internal energy of the acetyl radical; results are shown in Figure 6 at three energies.

The acetyl ground state PES has a TS. The forward unimolecular dissociation barrier height is well established as

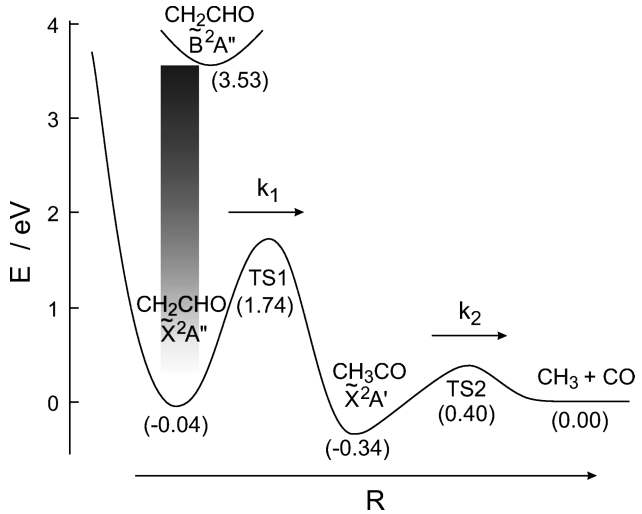

FIG. 5. Schematic potential energy surfaces of the vinoxy radical system leading to CH_3 and CO products. All energies are in eV, including zero-point energies and are relative to the product minimum (Ref. 18).

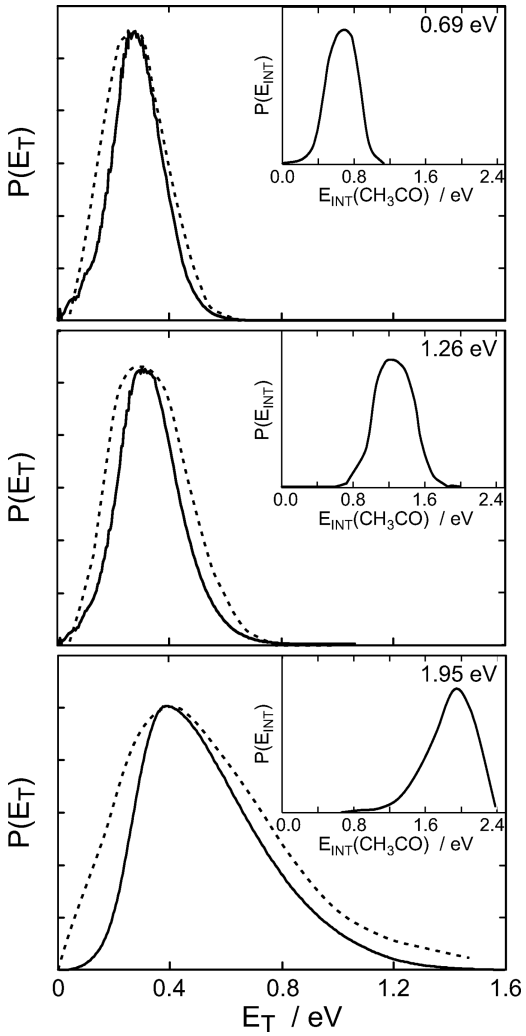

FIG. 6. Comparison of experimental (dashed) and calculated (solid) SAI $P(E_T)$ distributions for the dissociation of acetyl radicals. The acetyl parent internal energy distributions are reported in the upper right insert of each panel for average $E_{INT}(CH_3CO)$ = 0.69, 1.26 and 1.95 eV. Experimental curves are reproduced from Refs. 20 and 21.

0.74 eV[18,19,22,23] with respect to the acetyl radical. Based on $\Delta H_{f,0}(CH_3CO) = -0.026 \pm 0.003$ eV,[25] a barrier of 0.40 eV with respect to products is defined; this is in agreement with our own *ab initio* study.[18] The reaction coordinate for the elimination of methyl and carbon monoxide from the acetyl radical is shown in Figure 4. This TS occurs at an elongated C–C bond length (2.1 Å), shown in Figure 2(a). From Tables I and II it is clear that the geometry and frequencies of the methyl and carbon monoxide groups at the TS closely resemble that of the products,[26] however the CCO skeletal backbone at the TS is strongly bent (115°).

We apply our SAI model to investigate the physical processes involved in ground state acetyl unimolecular dissociation through this TS state (E^{TS}=0.40 eV) for internal energy distributions with an average $E_{INT}(CH_3CO)$=0.69, 1.26 and 1.95 eV. The geometry, frequencies and normal modes of the TS are obtained by electronic structure calculations at the QCISD/6-31G** level as described in Ref. 18; these compare favorably with the results in Ref. 23. The internal energy $P^{STAT}(E'_{INT})$ distribution for the statistical reservoir,

TABLE I. Geometries of acetyl dissociation and vinoxy-acetyl isomerization TS and asymptotic products.[a]

	Acetyl TS[b]	Vinoxy TS[b]	CH_3+CO[c]
r(C–O)	1.15	1.20	1.13
r(C–C′)	2.11	1.41	–
r(C′–H)	1.09	1.48	1.08
r(C′–H′)	1.09	1.08	1.08
r(C′–H″)	1.09	1.09	1.08
∠(C′CO)	115	139	–
∠(HC′C)	103	53	–
∠(H′C′C)	100	118	–
∠(H″C′C)	100	122	–
∠(HC′CO)	180	0	–
∠(H′C′CO)	−60	−69	–
∠(H″C′CO)	60	117	–

[a]Units: bond lengths are reported in Å and angle in degrees.
[b]Calculated at the QCISD/6-31G** level.
[c]Reported experimental geometries from Ref. 26.

Figure 7(a), is calculated from the projection of the TS vibrational modes onto the product modes; the asymptotic correlation of the TS vibrational modes required for calculation are given in Table II. The internal energy $P^{IMP}(E''_{INT})$ distribution for the impulsive reservoir, Figure 7(b), is calculated from the Franck-Condon vibrational distribution and impulsive model Figures 7(c) and 7(d). The geometry and frequencies used are reported in Table I and Table II. The resultant calculated SAI $P(E_T)$ distributions are compared with the experimental results, Figure 6.

The contribution from the impulsive reservoir consists of two components: the Franck-Condon vibrational distribution and the impulsive partitioning of rotational energy. The similar TS and product geometries and frequencies, Table I and Table II, result in low vibrational excitation in the products for the impulsive reservoir. Thus, the Franck-Condon vibrational distribution has only a few delta functions associated with a short progression in the ν_3 mode, with the largest intensity at E_{INT}=0 eV, Figure 7(c). The strongly bent CCO skeletal backbone of the TS results in a large impact parameter for the CO fragment; this generates a large degree of torque upon sudden dissociation which results in $\langle f_R \rangle \sim$ 0.35, i.e., ca. 35% of E^{IMP} being partitioned into rotational energy of the CO fragment. Combining these two components, the resultant $P^{IMP}(E''_{INT})$ distribution, Figure 7(b), contains mostly rotational excitation.

Photolysis of the acetyl halides produces acetyl radicals with internal energy distributions described by an average internal energy and a broad width; see the inserts in Figure 6. The average energies are 0.69, 1.26 and 1.95 eV, for dissociation of acetyl chloride,[19,20] bromide[20] and iodide[21] respectively. All acetyl radicals with an internal energy greater than the TS barrier ($E^{TS}+D_0$), undergo unimolecular dissociation and contribute to the CH_3 and CO product state distribution. These product state distributions are calculated for each parent internal energy above the TS barrier, and are summed (weighted by the parent internal energy probability distribution) to yield the final product distributions, as reported in Figure 6.

Comparison between experiment and the SAI model

TABLE II. Asymptotic correlation of TS vibrational modes for the unimolecular dissociation of the acetyl radical. The calculation for the TS is performed at the QCISD/6-31G** level, (Ref. 18) experimental frequencies (Ref. 26) are used for the products.

ν_{TS}/cm^{-1}	TS mode	$\nu_{Product}/cm^{-1}$	Product mode
3276	CH_3 asym. str. (a'')	3161	CH_3 asym. str. (e')
3260	CH_3 sym. str. (a')	3161	CH_3 sym. str. (e')
3105	H–CH_2 str. (a')	3004	H–CH_2 str. (a')
2044	CO str. (a')	2170	CO str. (a')
1453	CH_3 deform. (a'')	1396	CH_3 deform. (e')
1446	CH_3 deform. (a')	1396	CH_3 deform. (e')
939	C–C′H′H″ bend(a')	606	CH_3 umbrella (a'')
611	CH_3 sym. rocking (a')	$E_T(+E_R)$	Translation+Rotation
547	CH_3 asym. rocking (a'')	$E_T(+E_R)$	Translation+Rotation
277	C′–CO bend (a')	$E_R(+E_T)$	Rotation+Translation
43	CH_3 wag (a'')	$E_R(+E_T)$	Rotation+Translation
466*i*	C–C′ str. (a')	$E_T(+E_R)$	Translation+Rotation

simulations is favorable for three excitation energies ranging from 0.69 to 1.95 eV, Figure 6. The SAI distributions accurately predict the maximum intensity in the $P(E_T)$ distributions and broaden with increased acetyl internal energy. However, the SAI predicted distributions are narrower than the experimental data in all instances. This is most likely due to the experimental uncertainty in acetyl internal energy and angular momentum which is the input for the SAI model. For each photon energy the resultant $P(E_T)$ distributions are consistent with 65% of E^{IMP} partitioned directly into translational energy. From our calculation we can go further than the current experimental data, predicting the energy disposal within the products. Namely, the energy associated with the barrier is partitioned dynamically into a combination of product rotation and translation, not vibration. As the photon energy is increased the excess energy above the TS is partitioned into the statistical reservoir; thus the amount of vibrational excitation will increase dramatically, whilst the rotational distribution although effected will not show such a marked effect, as noted in the photodissociation of CH_3CHO[16] and HFCO.[27]

B. Photodissociation of vinoxy radicals

Photodissociation of the vinoxy (CH_2CHO) radical offers another example of nonstatistical behavior. The detailed paper by Osborn *et al.*[18] reports experimental and electronic structure calculations for the photodissociation of vinoxy via the $\tilde{B}(^2A'')-\tilde{X}(^2A'')$ absorption band. Two photodissociation channels are observed, with branching ratios ϕ_{I} and ϕ_{II}:

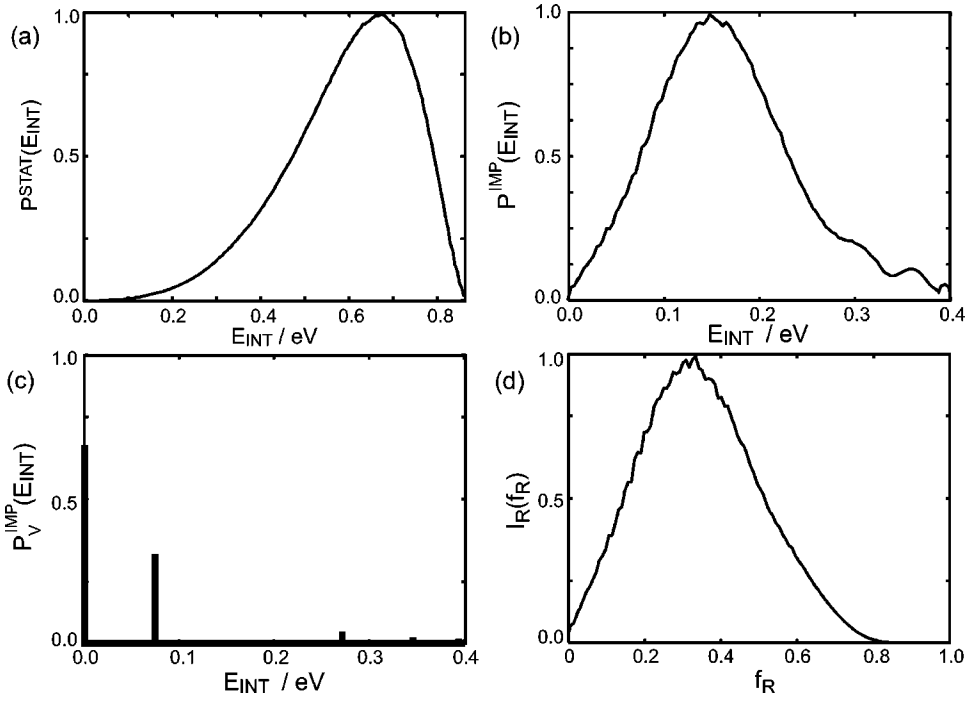

FIG. 7. Unimolecular dissociation of the acetyl radical. (a) The internal energy distributions for the statistical reservoir at $E^{STAT}=0.86$ eV. (b) The calculated internal energy distribution for the final impulsive reservoir, Eq. 7. (c) the Franck-Condon vibrational energy distribution Eq. 4. (d) Fraction of impulsive energy partitioned into rotational energy for the impulsive reservoir, Eq. 5.

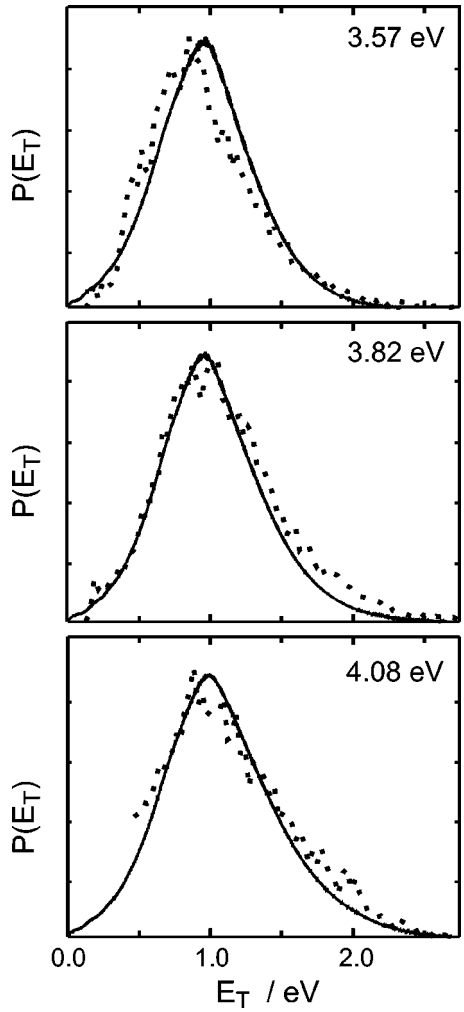

FIG. 8. Comparison of experimental (dashed) and calculated (solid) SAI $P(E_T)$ distributions for the dissociation of vinoxy radicals. Experimental curves are reproduced from Ref. 18.

I. $CH_2CHO+h\nu \rightarrow CH_3+CO \quad \phi_I \sim 20\%$

II. $CH_2CHO+h\nu \rightarrow CH_2CO+H \quad \phi_{II} \sim 80\%$.

Here we are concerned with channel I, as this dissociation proceeds over a large TS barrier. Channel II results from a competing dissociation mechanism. The experimental range in excitation energies is from 3.57 to 4.08 eV. In all cases, the form of the $P(E_T)$ distributions remains very similar, increasing from zero translational energy to a maximum intensity at $E_T \sim 0.9$ eV, and then decreasing with a near-exponential function extending to the maximum available energy, Figure 8.

Dissociation is believed to proceed via internal conversion from the initially prepared $\tilde{B}(^2A'')$ state forming a microcanonical ensemble of vibrational levels on the $\tilde{X}(^2A'')$ state. The energy profile along the reaction coordinate from the state vinoxy radical to methyl and carbon monoxide products is depicted in Figure 5. Two transition states exist. The first, the vinoxy-acetyl isomerization TS is calculated to lie 1.78 eV[18] above the $\tilde{X}(^2A'')$ state vinoxy minimum. This is a tight three-center TS defined by the 1,2 hydrogen shift. The potential energy barrier is created because of significant torsional distortion of the molecular orbitals and poor overlap of the migrating H atom with these orbitals. The second, the TS for elimination of CO, from acetyl is located 0.40 eV above the product exit channel, and is discussed in Section III A.

The two transition states divide molecular phase space into three distinct regions. However at our high photon energies ($h\nu \geqslant 3.57$ eV) the molecular phase space is significantly simplified. The RRKM rate constants for passage through each TS can be calculated,[5]

$$k_{\mathrm{RRKM}}(E)=\frac{N^{\ddagger}(E)}{h\rho(E)}, \tag{9}$$

where $N^{\ddagger}(E)$ is the number of TS modes orthogonal to the reaction coordinate, accessible at energy E, h is Planck's constant, and $\rho(E)$ is the density of states in the reactant reservoir. Both $N^{\ddagger}(E)$ and $\rho(E)$ are calculated using the Beyer-Swinehart algorithm and the vibrational frequencies reported in Table II, Table III and Ref. 18. The RRKM rate constants are reported in Table IV. As can be ascertained from these rates, many molecular vibrations occur before passing through the vinoxy-acetyl isomerization TS, clearly defining a dynamical bottleneck in phase space. However, passage through the acetyl-product TS is rapid (less than a

TABLE III. Asymptotic correlation of TS vibrational modes for the unimolecular dissociation of the vinoxy radical. The calculation for the TS is performed at the QCISD/6-31G** level (Ref. 18), experimental frequencies (Ref. 26) are used for the products.

$\nu_{TS}/\mathrm{cm}^{-1}$	TS mode	$\nu_{\mathrm{Product}}/\mathrm{cm}^{-1}$	Product mode
3276	C′H″H′ asym. str. (a'')	3161	CH_3 asym. str. (e')
3098	C′H″H′ sym. str. (a')	3161	CH_3 sym. str. (e')
1966	C′–H str. (a')	3004	H–CH_2 str. (a')
1846	CO str. (a')	2170	CO str. (a')
1465	C′H″H′ deform. (a'')	1396	CH_3 deform. (e')
1229	C-C′ str. (a')	$E_T(+E_R)$	Translation+Rotation
1126	C-H str. (a'')	$E_T(+E_R)$	Translation+Rotation
1036	C′H″H′ deform. (a')	1396	CH_3 deform. (e')
836	C–C′H″H′ bend (a'')	606	CH_3 umbrella (a'')
633	OC–H bend (a')	$E_R(+E_T)$	Rotation+Translation
438	C′–CO bend (a')	$E_R(+E_T)$	Rotation+Translation
1675*i*	H migration (a')	$E_T(+E_R)$	Translation+Rotation

TABLE IV. Calculated RRKM rate constants.

$h\nu$/eV	$1/k_1(h\nu)$/ fs	$1/k_2(h\nu)$/fs
4.08	4,520	24
3.82	6,470	26
3.57	9,630	29

typical vibrational period), hence this TS can be ignored at these photon energies. We are now in the original situation of unimolecular dissociation over one TS.

In addition, the TS is treated as a concerted dissociation rather than H atom migration followed by dissociation of the C–C bond, as the impulsive model can only be used to describe a sudden impulsive dissociation. Following Moore and coworkers,[28] the axis of the impulsive force for a concerted dissociation is best defined by examining the reaction coordinate at and beyond the TS via *ab initio* calculations. For vinoxy dissociation, two points define the impulsive axis: the center of mass of the newly formed C–H bond, and the point of the remaining C atom which completes the three-center TS, e.g., Figure 2(b). Our *ab initio* calculations indicate that, after passing through the TS geometry, the fragments are repelled by a strong potential gradient along this axis and dissociate rapidly without further large changes in geometry.

The SAI model is applied to predict the resultant $P(E_T)$ distributions. A microcanonical ensemble of vibrational states is considered in equilibrium with all parts of the vinoxy phase space, and forms a microcanonical ensemble of states at the vinoxy-acetyl TS. The statistical reservoir is projected onto the CH_3+CO products, utilizing the asymptotic correlation of TS frequencies in Table III. This yields the $P^{STAT}(E'_{INT})$ distribution, Figure 9(a). The internal energy $P^{IMP}(E''_{INT})$ distribution for the impulsive reservoir, Figure 9(b), is calculated from the Franck-Condon vibrational distribution and impulsive model Figures 9(c) and 9(d), the geometry and frequencies used are reported in Table I and Table III. The resultant calculated SAI $P(E_T)$ distributions is compared with the experimental results, Figure 8.

In general, for dissociation of a microcanonical ensemble through a TS, the statistical reservoir contribution, $P^{STAT}(E_{INT})$, has the same general form as the distributions for statistical unimolecular dissociation, e.g., Figure 7(a) and Figure 9(a). However, the partitioning of E^{IMP} between vibration and rotation is very sensitive to TS geometry even though the overall $P^{IMP}(E_{INT})$ distributions in Figure 7(b) and Figure 9(b) are similar. The large difference between TS and product geometry and frequencies for vinoxy, Table I and Table III, yields high vibrational excitation of the products for the impulsive reservoir, as in Figure 9(c). The elongated $H–CH_2$ bond length at the TS results in the $H–CH_2$ stretch being particularly active. Interestingly, the methyl group at the TS is almost planar creating only a small degree of vibrational excitation in the ν_3 modes of the methyl product from the impulsive reservoir. The CCO skeletal backbone angle for vinoxy TS is closer to linearity (139°) than that for acetyl dissociation, as reflected in the smaller impact parameter, 0.48 Å verses 0.59 Å for vinoxy and acetyl, respectively. The smaller impact parameter generates less torque upon sudden dissociation, which results in $\langle f_R \rangle \sim 0.23$. As the impact parameter of the methyl fragment is considerably smaller than that of the carbon monoxide all the

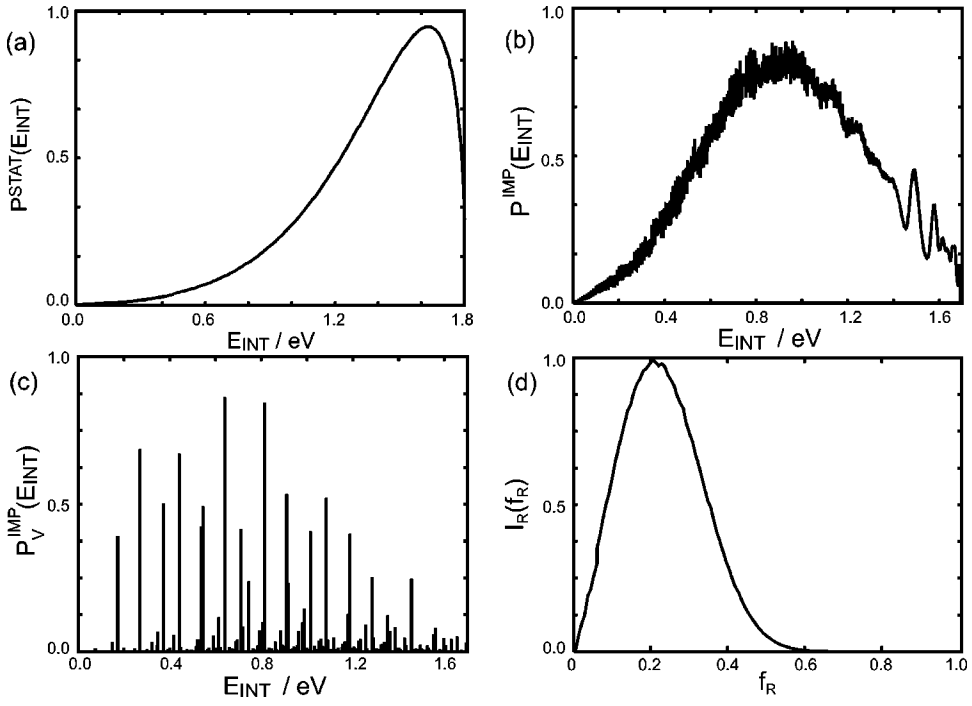

FIG. 9. Unimolecular dissociation of the vinoxy radical. Unimolecular dissociation of the acetyl radical. (a) The internal energy distributions for the statistical reservoir at $E^{STAT}=1.8$ eV. (b) The calculated internal energy distribution for the final impulsive reservoir, Eq. 7. (c) The Franck-Condon vibrational energy distribution Eq. 4. (d) Fraction of impulsive energy partitioned into rotational energy for the impulsive reservoir, Eq. 5.

rotational energy generated in the impulsive reservoir is partitioned into CO rotation. Combining these two components, the resultant $P^{IMP}(E''_{INT})$ distribution in Figure 9(b) contains mostly vibrational with some modest CO rotational excitation.

Again comparison between experiment and the SAI model simulations are favorable for a range in photon energies from 3.57 to 4.08 eV, Figure 8. For each photon energy the resultant $P(E_T)$ distribution are consistent with 60% of E^{IMP} partitioned directly into translational energy. Product vibration and rotation accounts for the remaining 40% of E^{IMP}. In this particular case, all product degrees of freedom are activated in the impulsive reservoir; energy in the statistical reservoir is also distributed among all the product degree of freedom, so no vibrational modes show activation with increasing photon energy above the TS. However, an interesting experimental quantity to measure would be the relative degrees of CH_3 and CO rotation; our model predicts that the majority of the rotational excitation created in the impulsive reservoir is partitioned into CO and not CH_3 rotation.

IV. CONCLUSION

A general framework is reported to simulate and interpret photodissociation processes in which internal conversion is followed by unimolecular dissociation over an exit barrier. The presence of a barrier along the reaction coordinate of the ground state surface forms a dynamical bottleneck, which divides phase space into reactant and product regions. The energy available to products can be divided into two independent reservoirs: statistical and impulsive energy reservoirs. The statistical reservoir considers direct projections of a vibrational microcanonical ensemble at the TS onto product quantum states, conserving vibrational adiabaticity and angular momentum. The impulsive reservoir considers the sudden dissociation of the zero-point TS wave function, with Franck-Condon and impulsive models. A convolution of this these two energy reservoirs yields the final product internal energy and translational energy distributions. We have derived the SAI model to predict the product translational distribution for nonstatistical dissociation over a barrier.

The photodissociation of acetyl and vinoxy radicals are considered as benchmark examples of nonstatistical dissociation over a barrier and their SAI product state distributions are presented. For both examples, approximately 60% of the barrier height is partitioned into translational energy. The only difference is that in the former case the SAI model predicts that most of the remaining energy goes into rotation, while in the latter case it goes into vibration; this is easily understood in terms of the TS geometries. This prediction could be tested by determining the product vibrational and rotational distributions, rather than the translational energy distribution, at energies close to the barrier height where the contribution from the statistical reservoir is small.

The SAI model predicts the product translational energy distributions for unimolecular dissociation over an exit barrier. Two factors have been determined to be important for nonstatistical dissociation over a barrier. First, the energy of the TS is predominantly partitioned into translational energy. Second, the geometry of the TS relative to that of products governs the degree to which the energy of the TS is partitioned into product rotational and vibrational energy. The results compare favorably with experiment for two molecular systems over a range of excitation energies. The model is not specific to the acetyl and vinoxy systems, but is general and should be applicable to most situations in which unimolecular dissociation occurs over an exit barrier.

ACKNOWLEDGMENTS

We are grateful to Professor Simon North for permission to compare his data with our SAI predictions. This research is supported by the Director, Office of Energy Research, Office of Basic Energy Sciences, Chemical Sciences Division of the U.S. Department of Energy under Contract No. DE-AC03-76SF00098.

[1] E. S. Yeung and C. B. Moore, J. Chem. Phys. **60**, 2139 (1974); C. B. Moore and J. C. Weisshaar, Annu. Rev. Phys. Chem. **34**, 525 (1983); W. F. Polik, D. R. Guyer, and C. B. Moore, J. Chem. Phys. **92**, 3453 (1990).
[2] M. Hunter, S. A. Reid, D. C. Robie, and H. Reisler, J. Chem. Phys. **99**, 1093 (1993).
[3] X. Zhao, R. E. Continetti, A. Yokoyama, E. J. Hinsta, and Y. T. Lee, J. Chem. Phys. **91**, 4118 (1989).
[4] D. H. Mordaunt, I. R. Lambert, G. P. Morley, M. N. R. Ashfold, R. N. Dixon, C. M. Western, L. Schnieder, and K. H. Welge, J. Chem. Phys. **98**, 2054 (1993).
[5] R. D. Levine and R. B. Bernstein, *Molecular Reaction Dynamics and Chemical Reactivity* (Oxford University Press, New York, 1987); R. D. Levine and J. L. Kinsey, *Atom-Molecule Collision Theory —A Guide for the Experimentalist*, edited by R. B. Bernstein (Plenum, New York, 1979).
[6] P. Pechukas and J. C. Light, J. Chem. Phys. **42**, 3281 (1965).
[7] C. Wittig, I. Nadler, H. Reisler, J. Catanzarite, and G. Radhakrishnan, J. Chem. Phys. **83**, 5581 (1985).
[8] D. G. Truhlar, B. C. Garrett, and S. J. Klippenstein, J. Phys. Chem. **100**, 12771 (1997).
[9] M. D. Morse, K. F. Freed, and Y. B. Band, J. Chem. Phys. **70**, 3604 (1979).
[10] G. E. Busch and K. R. Wilson, J. Chem. Phys. **56**, 3626 (1972); A. F. Tuck, J. Chem. Soc. Faraday Trans. **73**, 689 (1977).
[11] M. Quack and J. Troe, *Theoretical Chemistry*, **6b**, edited by D. Henderson (Academic, New York, 1981); J. Troe, *State-Selected and State-to-State Ion-Molecule Reaction Dynamics, Part 2: Theory*, edited by M. Bear and C. Y. Ng (Wiley, New York, 1992).
[12] I-C. Chen and C. B. Moore, J. Phys. Chem. **94**, 269 (1990).
[13] M. J. Berry, J. Chem. Phys. **61**, 3114 (1974).
[14] E. Zamir and R. D. Levine, Chem. Phys. **52**, 253 (1980).
[15] B. L. Sonobe, T. R. Fletcher, and R. N. Rosenfeld, J. Am. Chem. Soc. **106**, 4352 (1984).
[16] T. Gejo, M. Takayanagi, T. Kono, and I. Hanazaki, Chem. Phys. Lett. **218**, 343 (1994).
[17] S. W. North, D. A. Blank, J. D. Gezelter, C. A. Longfellow, and Y. T. Lee, J. Chem. Phys. **102**, 4447 (1995).
[18] D. L. Osborn, H. Choi, D. H. Mordaunt, R. T. Bise, D. M. Neumark, and C. M. Rohlfing, J. Chem. Phys. **106**, 3049 (1997).
[19] S. W. North, D. A. Blank, and Y. T. Lee, Chem. Phys. Lett. **224**, 38 (1994).
[20] S. W. North, Ph.D. thesis, University of California, Berkeley, 1995.
[21] P. M. Kroger and S. J. Riley, J. Chem. Phys. **67**, 4483 (1977).
[22] K. W. Watkins and W. W. Word, Int. J. Chem. Kinet. **6**, 855 (1974).
[23] S. Deshmukh, J. D. Myers, S. S. Xantheas, and W. P. Hess, J. Phys. Chem. **98**, 12535 (1994).
[24] R. Schinke, *Photodissociation Dynamics* (Cambridge University Press, Cambridge, 1993).
[25] J. T. Niiranen, D. Gutman, and L. N. Krasnoperov, J. Phys. Chem. **96**, 5881 (1992); C. W. Bauschlicher, Jr., *ibid.* **98**, 2564 (1994).

[26] K. P. Huber and G. Herzberg, *Molecular Spectra and Molecular Structure, IV. Constants of Diatomics Molecules* (Van Nostrand, Reinhold, 1979); M. W. Chase, Jr., C. A. Davies, J. R. Downey, Jr., D. J. Frurip, R. A. McDonald, and A. N. Syverud, J. Chem. Phys. Ref. Data **14**, Suppl. No. 1 (1985).

[27] C. L. Reed, M. Kono, S. R. Langford, R. N. Dixon, and M. N. R. Ashfold, J. Chem. Soc. Faraday Trans. **93**, 2721 (1997).

[28] R. D. van Zee, C. D. Pibel, T. J. Butenhoff, and C. B. Moore, J. Chem. Phys. **97**, 3235 (1992); D. J. Bamford, S. V. Filseth, M. F. Foltz, J. W. Hepburn, and C. B. Moore, *ibid.* **82**, 3032 (1985).